THE JOURNAL OF PHYSICAL CHEMISTRY A

Article

pubs.acs.org/JPCA

Time Resolved Photoelectron Spectroscopy of Thioflavin T Photoisomerization: A Simulation Study

Hao Ren, Benjamin P. Fingerhut, and Shaul Mukamel*

Department of Chemistry, University of California, Irvine, California 92617, United States

Supporting Information

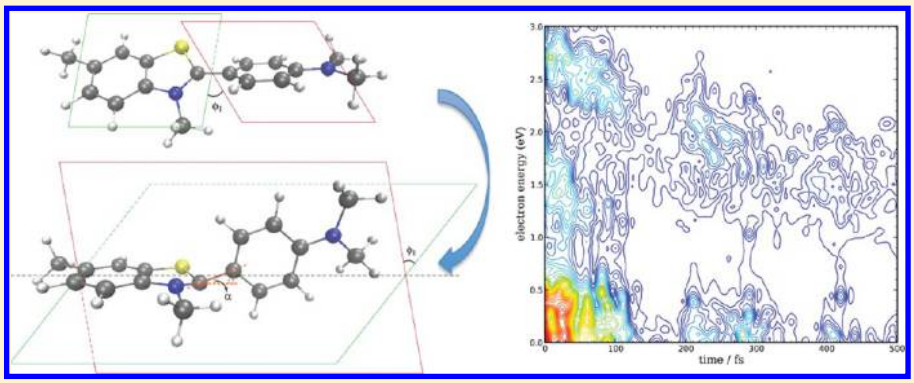

ABSTRACT: The excited state isomerization of thioflavin T (ThT) is responsible for the quenching of its fluorescence in a nonrestricted environment. The fluorescence quantum yield increases substantially upon binding to amyloid fibers. Simulations reveal that the variation of the twisting angle between benzothiazole and benzene groups (ϕ_1) is responsible for the subpicosecond fluorescence quenching. The evolution of the twisting process can be directly probed by photoelectron emission with energies $\varepsilon \geq 1.0$ eV before the molecule reaches the ϕ_1-twisted configuration (~300 fs).

1. INTRODUCTION

Amyloid fibrils are insoluble filaments formed by proteins with ordered, fibrous structures which share a common series of biophysical and structural properties.[1,2] The accumulation of amyloid fibrils in organism tissues can lead to a number of diseases, such as Alzheimer's and Parkinson's diseases and type II diabetes.[2−7] Detailed information about the fibrillation/aggregation dynamics of amyloid fibrils is required to reveal the fibrillation mechanism, and would be helpful to pathologically overcoming these diseases. Traditional analytical techniques, such as X-ray diffraction, are impractical for in vivo investigations. Thioflavin T (ThT) (see Figure 1), a benzothiazole dye, has been

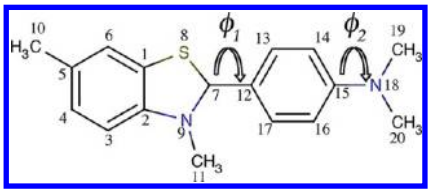

Figure 1. Geometry of thioflavin T. Twisting in the excited state occurs along ϕ_1 (around C7−C12 single bond) and ϕ_2 (around C15−N18).

used to detect the formation of amyloid fibrils, since it does not interact significantly with folded or unfolded protein monomers and its fluorescence quantum yield is enhanced by about 3 orders of magnitude upon binding to amyloids.[8]

Even though the use of ThT as an amyloid sensor has been known for over 50 years,[9−11] the photophysics associated with its fluorescence quenching and the binding mechanism with amyloid fibrils are not well understood. Recent experiments showed that ThT monomer binds to β-sheets such that its long axis is perpendicular to the β-strands.[10] The molecular rotor mechanism supported by both experiments and potential energy surface calculations is the most likely explanation of the fluorescence enhancement upon binding.[8,12] It assumes that the fluorescence is caused by a twisting of the benzothiazole and dimethylaniline groups around the C−C single bond in its first excited state. As shown in Figure 1, there are two possible twisting coordinates around the C−C and C−N single bonds, corresponding to the dihedral angles between the benzothiazole/benzene (ϕ_1) and benzene/dimethylamino (ϕ_2) groups. According to the potential energy surface calculation of Stsiapura et al.,[12] the rotational barrier for ϕ_2 is 4 times higher than that of ϕ_1; ϕ_1 is thus the more likely candidate. In the ground state S_0, the potential energy minimum is at $\phi_1 \sim 37°$, which is a consequence of the π-electron conjugation and the steric effect between the benzothiazole methyl group and the benzene H atom. However, in the first excited state S_1, which is

Special Issue: Prof. John C. Wright Festschrift

Received: January 2, 2013
Revised: March 19, 2013
Published: March 21, 2013

dx.doi.org/10.1021/jp400044t | J. Phys. Chem. A 2013, 117, 6096−6104

responsible for the fluorescence, the stable configuration has $\phi_1 \sim 90°$. Stsiapura et al. proposed that the molecule is photoexcited to its first Franck−Condon locally excited (LE) state and then exhibits an ultrafast twisting to its excited state minima, during which charge transfer to the benzothiazole group occurs.[12] The fluorescence from the twisted intramolecular charge transfer (TICT) state is very weak.

The LE → TICT ultrafast excited state dynamics is affected by the friction due to solvent; thus the fluorescence lifetime and quantum yield strongly depend on solvent viscosity or the rigidity of the microenvironment when binding to amyloid fibrils.[13,14] Subpicosecond fluorescence lifetime in low-viscosity solutions extends to tens of picoseconds in highly viscous solutions.[8,15,16] Huppert el al. found a linear decrease of the excited state decay rate with solvent viscosity.[17] There is little difference between steady state emission maxima of ThT in polar and nonpolar solvents.[8,16]

In this paper, we present a simulation of the twisting isomerization dynamics of ThT in S_1 in aqueous solution and how it may be probed by time resolved photoelectron spectra (TRPES). TRPES has been proven to be an valuable technique for the analysis of the photophysics and photochemistry of molecules in their excited states.[18−20] Recent developments of photoelectron techniques in liquid phase had extended TRPES to solutions.[21−23] TRPES can reveal the details of the excited state isomerization and the fluorescence quenching mechanism of ThT. We find that the twisting angle ϕ_1 can be directly revealed by the kinetic energy of the high energy (≥1.0 eV) photoelectrons before it reaches its TICT state. Details of isomerization dynamics and photoelectron simulation protocol are given in section 2. The results are presented in section 3 and summarized in section 4.

2. SIMULATION PROTOCOL

2.1. Isomerization Dynamics. Excited state isomerization dynamics is performed using ab initio molecular dynamics trajectories implemented in the Newton-X package.[24,25] In preparing the initial states for the dynamics simulation, nuclear motions are treated as harmonic. The initial coordinates and velocities are generated by random sampling according to the Wigner distribution for quantum harmonic oscillators.[24,25] We used time-dependent density functional theory (TDDFT) with the B3LYP functional and DZP basis set implemented in the TURBOMOLE package[26] to describe the electronic structure. TDDFT is fast and analytical excited state gradients are available. TDDFT with nonlocal hybrid density functionals has been successfully used on the excited state twisting dynamics in good agreement with experiments.[27−30]

Thirty-six initial configurations of the first excited state are prepared for the 800 fs excited state dynamics simulation with 1 fs time step. The TDDFT dynamics break down when the molecule encounters a geometry that involves multireference character.[28] These events are rare for times shorter than 500 fs;[31] we thus limited our study to this time regime.

2.2. Photoelectron Transition Probability. In a time-dependent photoelectron process, the molecule is pumped into an excited state and after a variable time delay t is ionized by a short probe pulse with frequency $\hbar\omega_p$.[19] It contains a single time delay together with the photoelectron energy and provides a two-dimensional (2D) representation of the signals. Allowing the system to interact with a sequence of ultrafast pulses could extend this technique to higher dimensions.[32] We assume that the ionization process is fast and vertical; i.e., geometry is preserved during electron ejection. The electronic wave function of the ionized system is written as $|\Psi_\alpha^{N-1}\Psi^\eta\rangle$, where η represents the ejected electron and N is the total number of electrons in the initial system. Within the dipole approximation, the photoelectron transition probability from the core state C is written as[19,33−35]

$$A_C^{N\to N-1}(t) \propto \sum_\eta A_{\eta C}^{N\to N-1} \tag{1}$$

where

$$A_{\eta C}^{N\to N-1} \propto |\langle\Psi^N|\hat{\boldsymbol{\mu}}|\Psi^{N-1}\Psi_C^\eta\rangle|^2 \delta(\hbar\omega_p + V^N(\boldsymbol{R}(t)) - V^{N-1}(\boldsymbol{R}(t)) - \varepsilon(\eta)) \tag{2}$$

Here $\hat{\boldsymbol{\mu}}$ is the electronic dipole operator. V^N and V^{N-1} are the potential energies of the N and $(N-1)$-electron systems, respectively, corresponding to the nuclear configurations $\boldsymbol{R}(t)$. $\varepsilon(\eta)$ is the photoelectron kinetic energy. The transition dipole matrix elements can then be written as

$$|\langle\Psi^N|\hat{\boldsymbol{\mu}}|\Psi_C^{N-1}\Psi^\eta\rangle|^2 = \left|\sum_{a,b}\langle\Psi^N|\hat{c}_a^\dagger\hat{c}_b|\Psi_C^{N-1}\Psi^\eta\rangle\langle\Psi_a|\hat{\boldsymbol{\mu}}|\Psi_b\rangle\right|^2 = \left|\sum_p\langle\Psi^N|\hat{c}_p^\dagger|\Psi_C^{N-1}\rangle\boldsymbol{\mu}_{p\eta}\right|^2 \tag{3}$$

where a and b label bound and scattering orbitals, respectively. We ignore the polarization of the probe beam and the angular distribution of photoelectrons, and replace the dipole matrix element $\boldsymbol{\mu}_{p\eta}$ by its rotationally averaged value μ_η. The transition dipole matrix is then factorized into a term governed by the difference between electronic structures of the N-electron initial state and the $(N-1)$-electron final state, and a term associated with the photoelectron kinetic energy, which we assumed to be a constant.[19,36]

$$|\langle\Psi^N|\hat{\boldsymbol{\mu}}|\Psi_C^{N-1}\Psi^\eta\rangle|^2 = \left|\sum_p\langle\Psi^N|\hat{c}_p^\dagger|\Psi_C^{N-1}\rangle\right|^2 \mu_\eta^{\,2} \tag{4}$$

The time resolved photoelectron signal for a given core state is obtained by summing over all the final states with the selected kinetic energy ε.

$$A_C^{N\to N-1}(\varepsilon, t) \propto \left|\sum_p\langle\Psi^N|\hat{c}_p^\dagger|\Psi_C^{N-1}\rangle\right|^2 \mu_\eta(\varepsilon)^2\,\rho(\varepsilon) \times \delta(\hbar\omega_p + V^N(\boldsymbol{R}(t)) - V^{N-1}(\boldsymbol{R}(t)) - \varepsilon(\eta)) \tag{5}$$

where $\rho(\varepsilon)$ is the density of states of scattered electrons. The product $\mu_\eta(\varepsilon)^2\,\rho(\varepsilon)$ in the low energy region only weakly depends on the kinetic energy, since $\mu_\eta(\varepsilon)^2$ decreases and density of states $\rho(\varepsilon)$ increases.[37]

$$A_C^{N\to N-1}(\varepsilon, t) \propto \left|\sum_p\langle\Psi^N|\hat{c}_p^\dagger|\Psi_C^{N-1}\rangle\right|^2 \times \delta(\hbar\omega_p + V^N(\boldsymbol{R}(t)) - V^{N-1}(\boldsymbol{R}(t)) - \varepsilon(\eta)) \tag{6}$$

The total signal is finally obtained by summing over the accessible core states C.

$$A^{N\to N-1}(\varepsilon, t) = \sum_C A_C^{N\to N-1}(\varepsilon, t) \tag{7}$$

dx.doi.org/10.1021/jp400044t | J. Phys. Chem. A 2013, 117, 6096−6104

3. RESULTS AND DISCUSSION

3.1. Geometries and Electronic Structure. The geometry and electronic structure of the states involved in the evolution are calculated on the (TD)DFT/B3LYP level with 6-311++G(d,p) basis set implemented in the Gaussian 09 package.[38] The optimized geometries in the ground and first excited states are shown in Figure 2. At the ground state minima, the molecule is twisted with $\phi_1 = 37.6°$, and the benzene and the dimethylamino are coplanar with $\phi_2 = 0.0°$. The twisted conformation in the ground state is due to the steric interaction between the N−CH_3 group and a nearby benzene H atom. The molecule twists further to $\phi_1 = 91.7°$ and $\phi_2 = 11.6°$ in the first excited state, and the long axis is also bent here. We define the bending of the long axis with the angle α between the C7−C12 single bond and the benzthiazole plane as shown in Figure 2b.

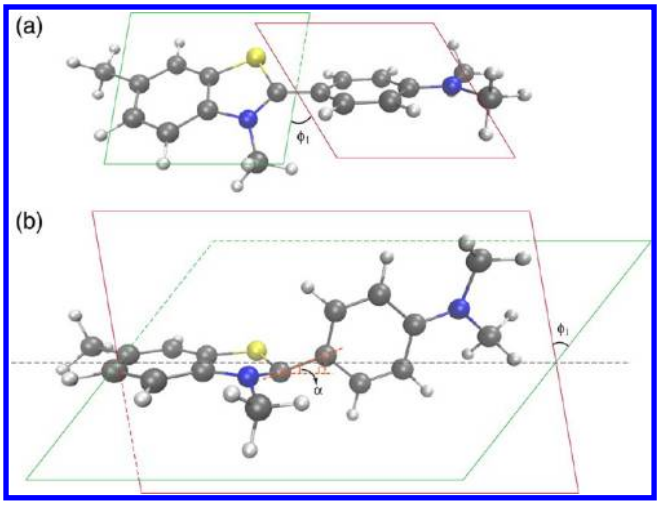

Figure 2. Optimized (a) ground state (S_0) and (b) first excited state (S_1) structures. The dimethylaniline in the ground state minimum ($\mathbf{R}_0$) is planar with $\phi_2 = 0.0°$. The long axis of the molecule is straight in $\mathbf{R}_0$ and is bent with an angle of $\alpha = 24.6°$ in $\mathbf{R}_1$. The dimethylaniline group is twisted with $\phi_2 = 11.6°$ in $\mathbf{R}_1$.

Figure 3 depicts the frontier orbitals and natural transition orbitals (NTO)[39] of the ThT first electronic transition in its ground and first excited state minima. In the ground state minimum (Figure 3, left panel, $\mathbf{R}_0$), the compositions of the highest occupied molecular orbital (HOMO)/hole and lowest unoccupied molecular orbital (LUMO)/electron orbitals are almost the same, indicating that the first electronic excitation is dominated by the HOMO−LUMO transition. The transition has clear π−π^* character, where all the orbitals presented are delocalized across the molecule; strong π conjugation effect is expected although the structure deviated from planar conformation. The first electronic excitation at the excited state minimum (Figure 3, right panel, $\mathbf{R}_1$) is also dominated by the HOMO−LUMO transition. However, both HOMO and LUMO orbitals are now localized in either the dimethylaniline or the benzothiazole group, indicating considerable charge transfer from dimethylaniline to benzothiazole during the photoexcitation. The π conjugation is broken at the perpendicular ($\phi_1 \sim 90°$) configuration. In the HOMO of $\mathbf{R}_1$, the state remains delocalized in the dimethylaniline group although the geometry deviates from planar configuration.

3.2. Excited State Isomerization Dynamics. Previous potential energy surface calculations showed no barrier from $\mathbf{R}_0$ to $\mathbf{R}_1$ for the S_1 state.[12] This implies a possible ultrafast evolution from the dipole-allowed (strong fluorescence) configuration to a dipole-forbidden (nonfluorescence) twisted configuration.[12]

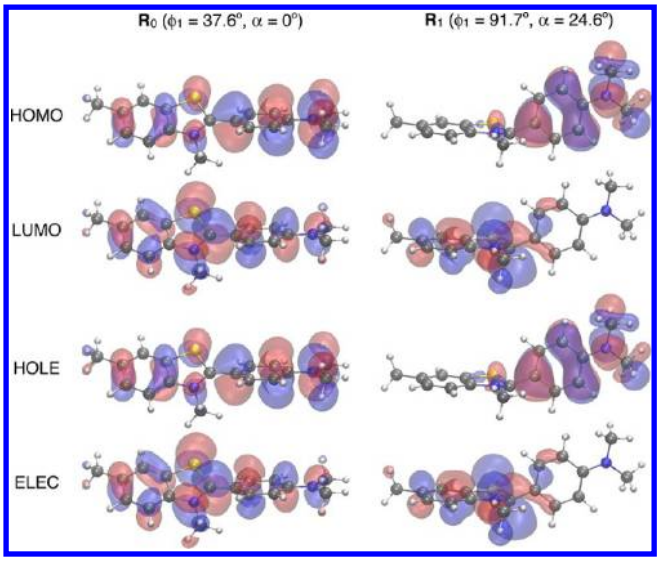

Figure 3. The 0.02 au isosurfaces of frontier orbitals (HOMO/LUMO) and natural transition orbitals (HOLE/ELEC) of ThT at its ground state ($\mathbf{R}_0$) and first excited state ($\mathbf{R}_1$) optimized goemetries.

Figure 4 shows the time-dependent geometry and electronic properties averaged over the trajectories used in the simulation. Figure 4a displays the evolution of the twisting angles and the bending angle . ϕ_1 varies from 37° at $t = 0$ fs to ∼100° in 400 fs. ϕ_2 also varies significantly: initially it is in the range −45−30°, changing to 15−25° after 400 fs. As found in previous calculations,[8,12] the S_1 state potential energy curve along ϕ_2 has a ∼3000 cm^{-1} barrier at $\phi_2 = \pm 60°$, which is much higher than that of ϕ_1 (∼700 cm^{-1}). The dimethylaniline group is not planar in the S_1 potential energy minima as shown in Figure 2b, where $\phi_2 = 11.6°$. ϕ_2 varies by ∼10° after 400 fs. We conclude that the variation of ϕ_2 during the evolution is the consequence of the random choice of nuclear coordinates and velocities, which drive ϕ_2 to oscillate in the potential energy well with $|\phi_2| < 50°$. The evolutions of ϕ_1 and ϕ_2 are related to their vibrational modes: the 96.4 cm^{-1} (at $\mathbf{R}_0$) twisting mode between benzothiazole and benzene for ϕ_1 and the 85.8 cm^{-1} (at $\mathbf{R}_0$) twisting mode between benzene and dimethyamino for ϕ_2. The molecule bends from straight to 20−25° after 400 fs evolution, and the bending angle α continues to increase thereafter. The slower variation of α is a consequence of the fact that it is related to the 32.2 cm^{-1} (at $\mathbf{R}_0$) bending mode.

The Mulliken charge distribution on the three parts of the molecule is shown in Figure 4b. This reveals a substantial charge transfer from dimethylamino to benzothiazole, where the charge population on the benzene group only varies slightly. The charge transfer is caused by electronic localization on benzothiazole during the twisting as shown in Figure 3. Figure 4c shows that the energy gap reduces from 3.0 to 1.0 eV in 500 fs, and does not lead to degeneracy of these states. The oscillator strength of the S_1−S_0 transition shown in Figure 4d rapidly decreases from 0.8 to below 0.2 in 100 fs, and further reduces to less than 0.1 after 300 fs. This suggests that, in unrestricted environments, the subpicosecond fluorescence quenching is mainly due to the ϕ_1 twisting. ThT evolves to a dipole-forbidden state in

dx.doi.org/10.1021/jp400044t | J. Phys. Chem. A 2013, 117, 6096−6104

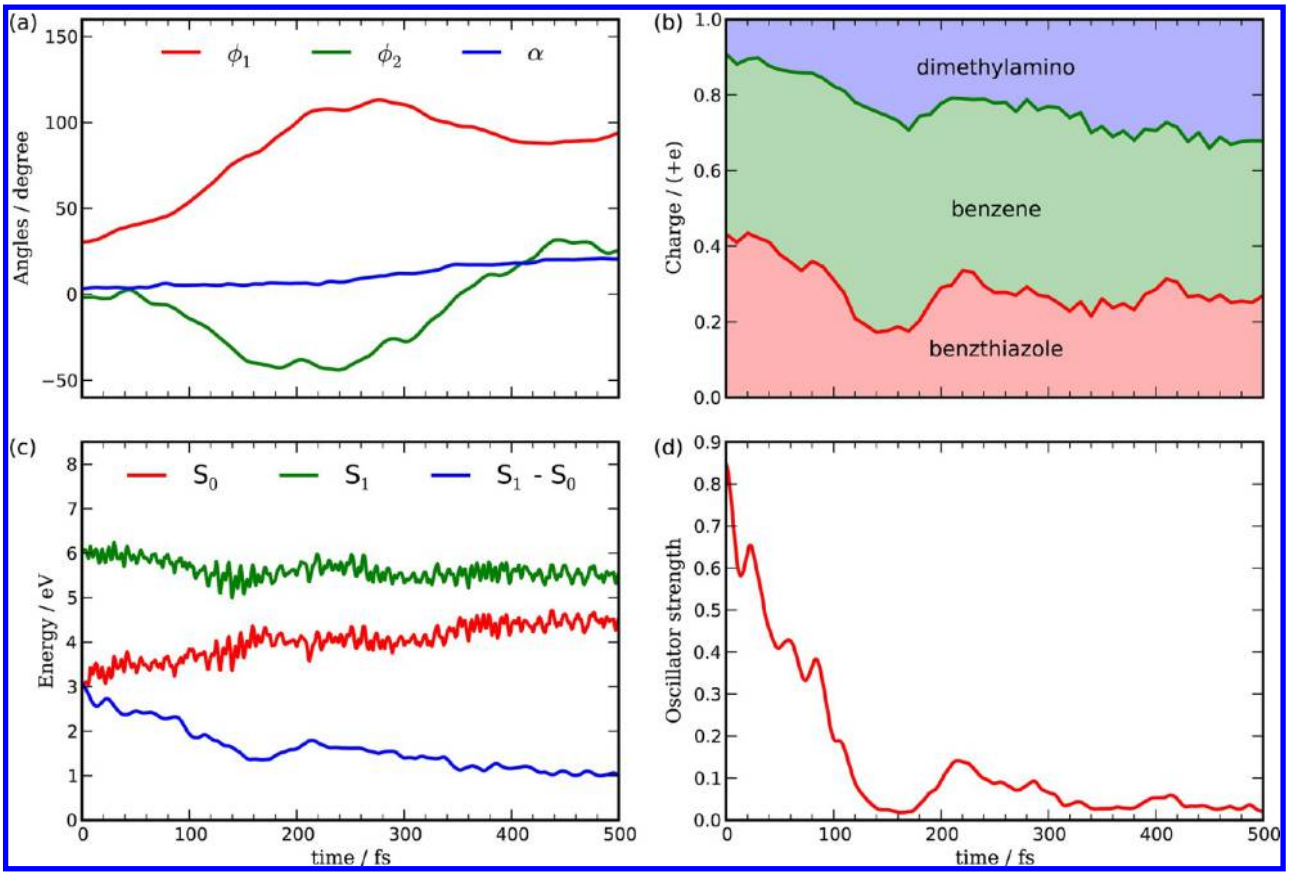

Figure 4. Time evolution of (a) twist angles and bending angle, (b) Mulliken charge populations in various regions, (c) energy gaps between S_1 and S_0, and (d) $S_1 \leftarrow S_0$ oscillator strengths. All panels are averaged over 29 trajectories.

400−500 fs, before encountering the conical intersection between S_0 and S_1.

3.3. Time Resolved Photoelectron Spectra. TRPES can monitor the evolution of electronic structure in the excited state. We have simulated the TRPES signals of ThT induced by a resonant pump that suddenly excites the molecule from S_0 to S_1 followed by a 125 nm (9.93 eV) UV ionization probe after a variable time delay t. We tuned the probe frequency so that only the first few lowest ionized states are accessible (~2.5 eV higher than the ionization threshold). TRPES were calculated at 10 fs intervals. Core states with energies higher than −10.0 eV are taken into account in the summation in eq 7.

Figure 5 depicts the time and energy resolved TRPES spectrum for a single trajectory. Vertical slices with t = 0, 100, 200, and 400 fs are shown in the top panels. The peaks are assigned to various ionization channels. The strongest features appear in the low electron energy regime at short decays. This indicates that higher excited states of the ionized molecule are generated in this regime. Since the photoelectron energy is related to the difference between the probe frequency and the ionization potential for the ionization channel, the lower energy region corresponds to higher excited states in the ionized molecule. The t = 0 fs slice is dominated by channels D_4 and higher. The weaker features at 2.93, 2.03, and 1.42 eV correspond to channels D_0, D_1, and D_2, respectively. In all channels the signals are dominated by the ionization of the outmost electron in the S_1 state, which is an open-shell singlet with the same ionization probability for α and β electrons. We have only calculated the ionization probability from α orbitals in S_1, which can be factorized into spin-polarized contributions from final states with different spins.

$$
\begin{aligned}
A_{C,p=\mathrm{HOMO}} &= \left|\langle \Psi^N | \bar{c}^{\dagger}_{p=\mathrm{HOMO}} | \Psi^{N-1} \rangle\right|^2 \\
&= |\langle \Psi^N_{\alpha} | \Psi^{N-1}_{\alpha} \rangle|^2 \left|\langle \Psi^N_{\beta} | \bar{c}^{\dagger}_{p=\mathrm{HOMO}} | \Psi^{N-1}_{\beta} \rangle\right|^2 \\
&= |S_{\alpha}|^2 |S_{\beta}|^2
\end{aligned} \tag{8}
$$

Here S_α and S_β are the overlap matrices between the α spin orbitals in S_1 with the α and β spin orbitals in D_n, respectively. As shown in Figure 6, the β states of the ionized molecule (Figure 6, right) have the same spatial distribution with the N-electron system (Figure 6, left), which results in a large S_β value near 1. However, the α states of S_1 (Figure 6, middle) have different symmetry from the N-electron system, although in both systems the states are delocalized among the whole molecule; the overlap S_α = 0.015, which is much smaller than $S_\beta \sim 1$. For channels D_1, D_2, and D_4, where the final states are the first, second, and fourth excited states of the ionized molecule, respectively, these three final states have considerable contribution from th e75$\alpha \rightarrow$ 76α transition in the configuration interaction (CI) expansions. S_β has the same value in the transition $D_0 \leftarrow S_1$, but S_α is much larger since the 76α state has a similar spatial distribution and symmetry compared with the 76th un-ionized state. Hence the intensities of the D_1, D_2, and D_4 channels only depend on the CI expansion coefficient of the 75$\alpha \rightarrow$ 76α transition. D_4 has the most 75$\alpha \rightarrow$ 76α component and is the strongest.

The time slices in Figure 5 show that the $D_0 \leftarrow S_1$ channel has similar intensities in the first 200 fs and decays by half at t = 400 fs.

dx.doi.org/10.1021/jp400044t | J. Phys. Chem. A 2013, 117, 6096−6104

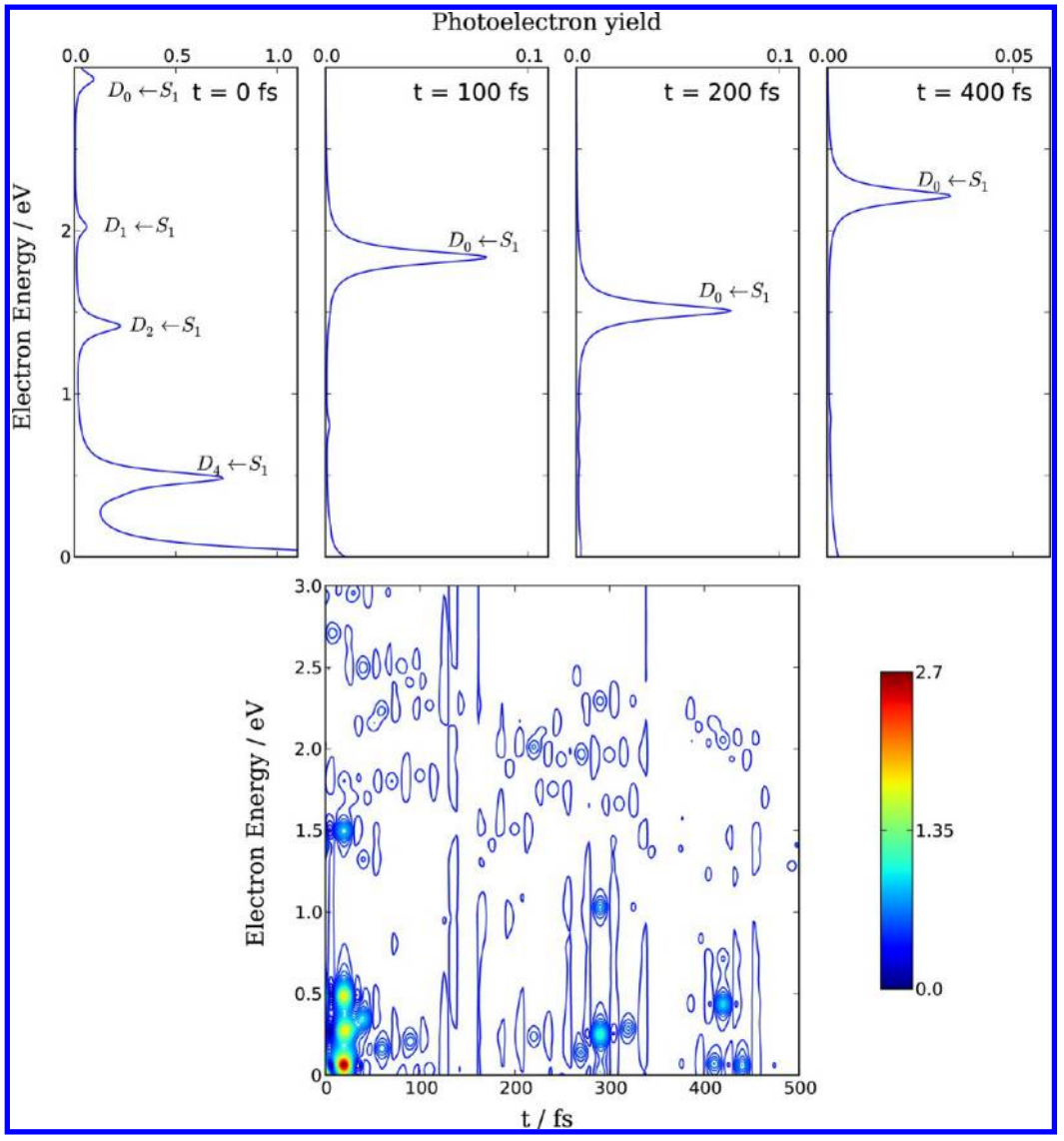

Figure 5. TRPES for a single trajectory. Top, vertical slices at t = 0, 100, 200, and 400 fs. Peaks are assigned to various ionization channels as marked.

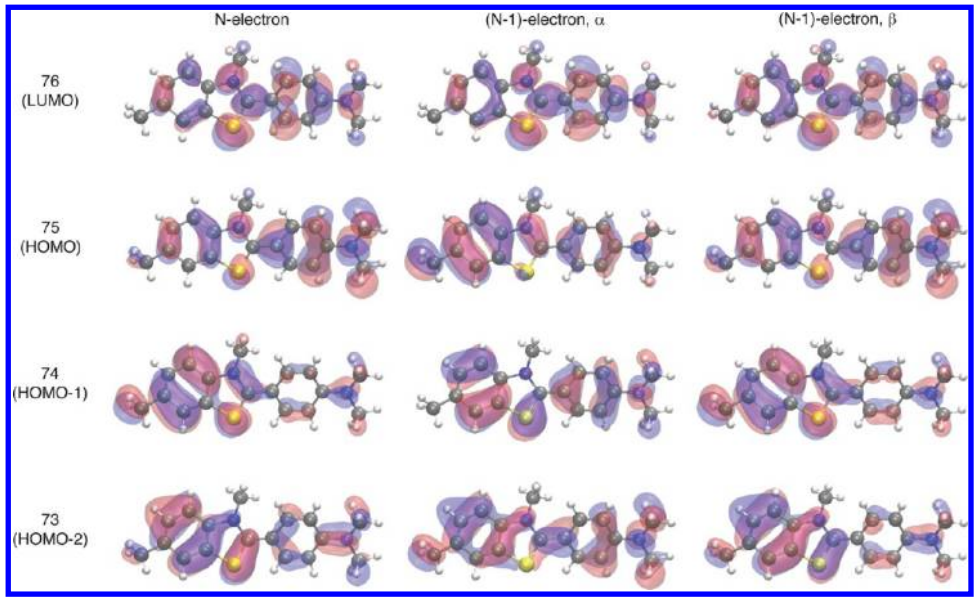

Figure 6. The 0.02 au isosurfaces the (left) N-electron, (middle) $(N-1)$-electron α, and (right) $(N-1)$-electron β frontier orbitals at t = 0 fs for the same trajectory used in Figure 5.

dx.doi.org/10.1021/jp400044t | J. Phys. Chem. A 2013, 117, 6096−6104

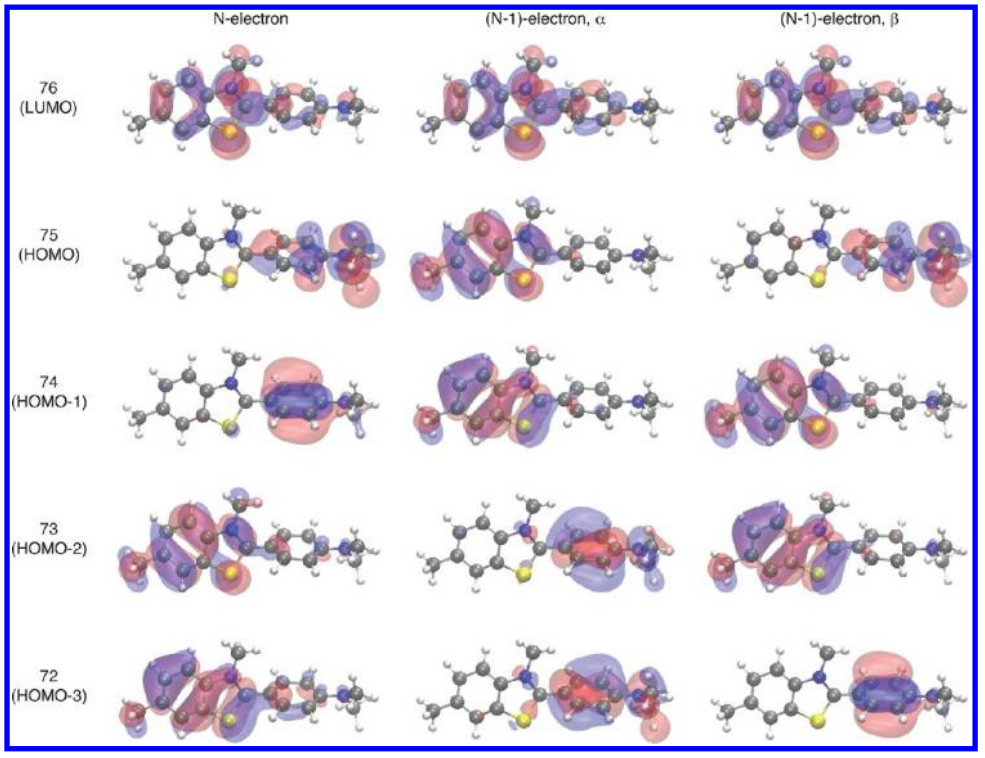

Figure 7. Same as Figure 6 except t = 200 fs.

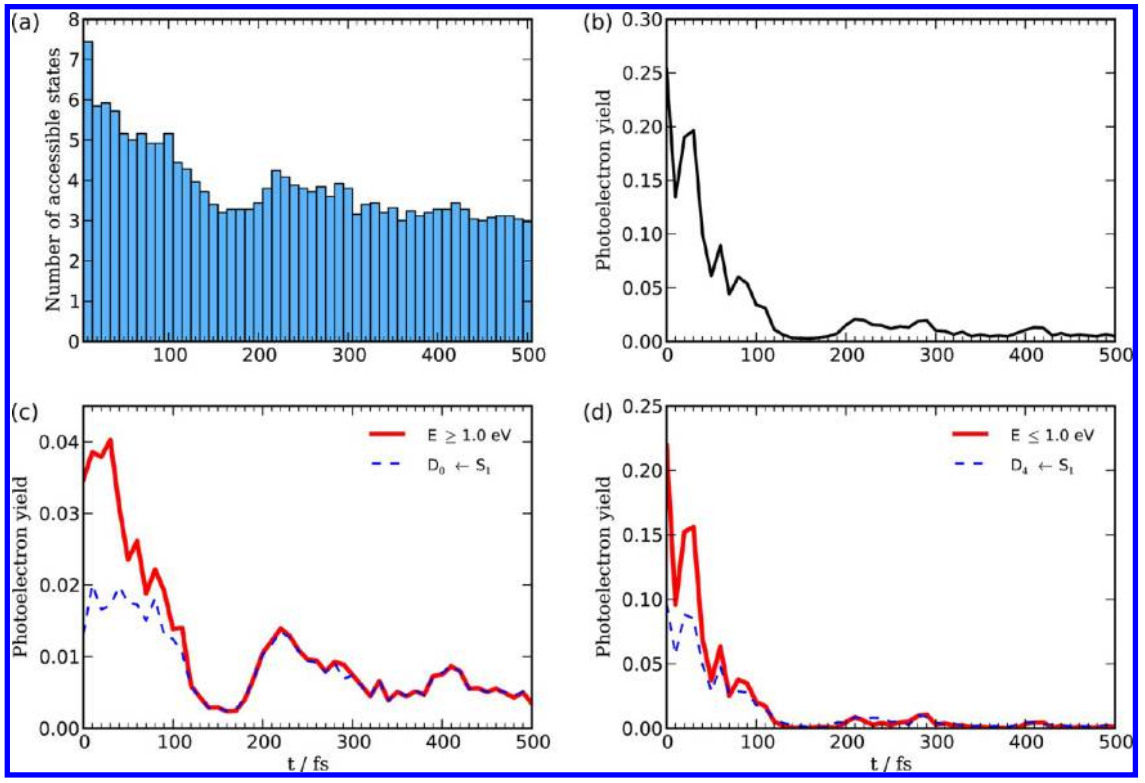

Figure 8. Time evolution of (a) number of ionized states accessible by the 125 nm probe, (b) energy integrated photoelectron probabilities, (c) high electron energy ($E \geq 1.0$ eV, solid) and $D_0 \leftarrow S_1$ probabilities (dashed), and (d) low electron energy ($E \leq 1.0$ eV, solid) and $D_4 \leftarrow S_1$ probabilities (dashed). All figures are averaged over 29 trajectories.

At t = 200 fs as shown in Figure 7, all the occupied orbitals are localized and the LUMO (76) state is delocalized. The S_1 excitation is dominated by the 75−76 transition. For $D_0 \leftarrow S_1$, the state pairs 72−73β, 73−74β, and 74−72β have similar symmetries and spatial distributions, although their orders are changed. This results in a large $S_\beta \sim 1$. Due to the delocalized distribution of state 76, the α overlap S_α = 0.012, comparable with that at t = 0 fs. However, all the channels ending in excited ionized states decay rapidly. This is a consequence of state localization caused by twisting during time evolution. At 200 fs, all the excited

dx.doi.org/10.1021/jp400044t | J. Phys. Chem. A 2013, 117, 6096−6104

ionized states accessible by the ionization probe only contain β transitions, which result in $S_\beta \sim 0$.

Figure 8a shows that the average number of states accessible by the ionization probe decreases from seven to eight at $t = 0$ fs to five to six in 100 fs, and further decreases to three to four after 300 fs. The integrated photoelectron yield shows similar behavior: it decays from 0.25 at $t = 0$ fs to 0.04 at $t = 100$ fs, and further decays to 0.01 after 400 fs. The TRPES features shown in Figure 9 can be divided into three groups. In the first 100 fs,

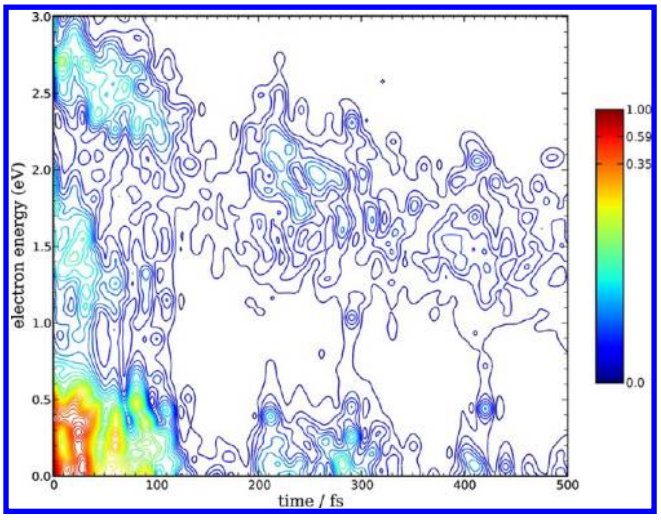

Figure 9. Time resolved photoelectron spectra averaged over 29 trajectories. The signals are shown on a nonlinear scale $\overline{S}$ = arcsinh(CS), where C is a constant making $\overline{S}$ near 1, for better visibility.

the three groups correspond to electron energies in the range 2.0−3.0, 1.0−2.0, and 0−1.0 eV. Strong signals for the low energy group in the first 100 fs are mainly contributed by the ionization channel $D_4 \leftarrow S_1$ as shown in Figures 8d and 10a−c. The ionization to D_4 rapidly decays to near zero after 100 fs. The features with electron energies 1.0−2.0 eV are mainly contributed by the ionization channels $D_1 \leftarrow S_1$, $D_2 \leftarrow S_1$, and $D_3 \leftarrow S_1$. These features also decay rapidly to near zero after 100 fs. The intensity decay is accompanied by decreasing of electron energies, and these features can appear in the lower energy region. For instance, there is a significant contribution from channel $D_3 \leftarrow S_1$ at $t = 200$ fs and $t = 400$ fs, as shown in Figure 10. The high energy peak intensities do not decay as fast as those of the lower energy groups. These come from channel $D_0 \leftarrow S_1$, with intensities only decaying by half from ∼0.02 at $t = 0$ fs to ∼0.01 after 400 fs. This is the consequence of the similar electronic configurations of the D_0 and S_1 states. The photoelectron energies decrease from 2.5−3.0 eV at $t = 0$ fs to 1.4−2.2 eV at $t = 400$ fs. Moreover, as shown in Figure 10, the energy distribution becomes broader during time evolution. This can be rationalized since the trajectories are initiated from random nuclear velocities and coordinates near $\mathbf{R}_0$. As the excited state gradient drives the evolution of nuclei, trajectories with different initial conditions might apart from each other on the potential energy surface; hence the photoelectron energies split as the system evolves.

The correlation scatter plot of the D_0 photoelectron energy and the ϕ_1 twisting angle is shown in Figure 11. In the early stage of the evolution (i.e., $t \leq 100$ fs), the $\varepsilon(D_0)$−ϕ_1 pairs locate near the line $\varepsilon(D_0) = -0.258\phi_1 + 9.71$, with an uncertainty $\Delta\phi_1 = \pm 5°$ for a specific D_0 energy. After 200 fs, the D_0 energies increase at ϕ_1 apart from 90°, which correspond to the S_1 state minima. Between 200 and 300 fs, there is also a linear relation $\varepsilon(D_0) = 0.258\phi_1 - 21.07$, with an uncertainty $\Delta\phi_1 = \pm 12°$. The uncertainty in determining ϕ_1 twisting angles through the high energy region peak positions comes from the perturbation by other geometry parameters, such as ϕ_2 and α. As shown in Figure 4 a, ϕ_2 varies on the same time scale as ϕ_1, but α increases much slower. That means that, in the early stage of evolution ($t \leq 200$ fs), the uncertainty is mainly attributed to

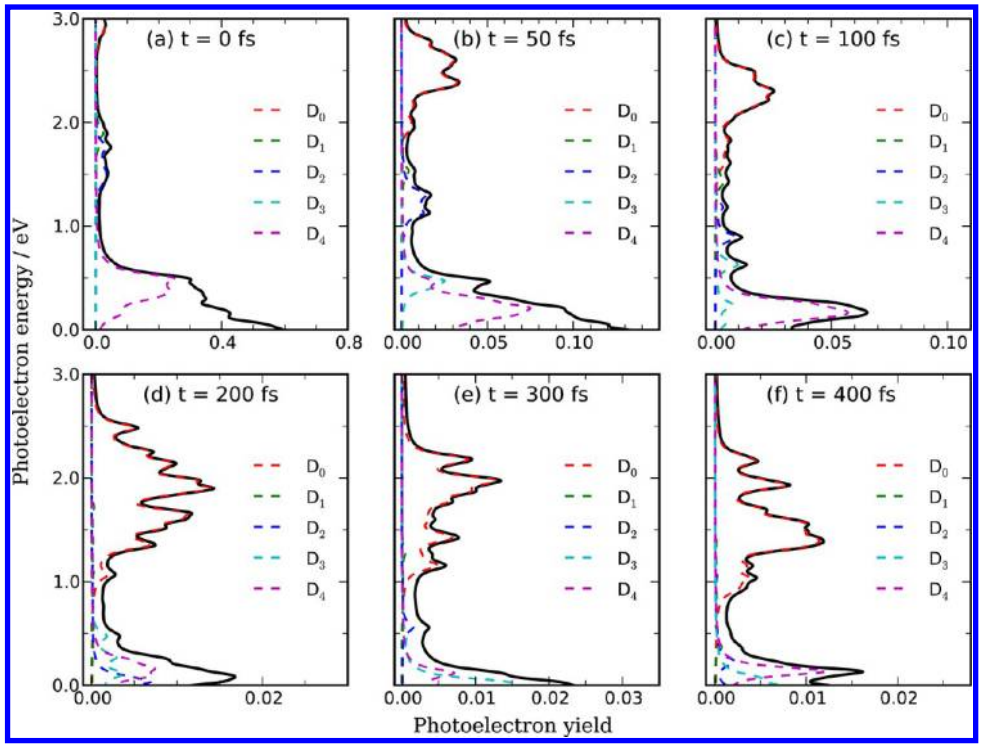

Figure 10. Solid lines: slices of Figure 9 at various times. Dashed lines: ionization channel resolved spectra.

dx.doi.org/10.1021/jp400044t | J. Phys. Chem. A 2013, 117, 6096−6104

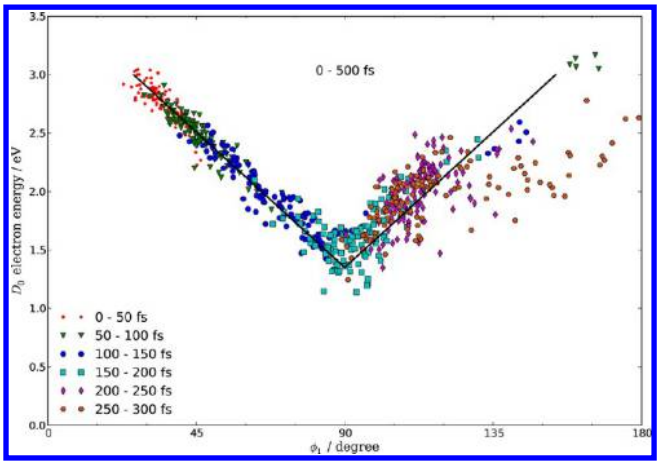

Figure 11. Correlation between the $D_0 \leftarrow S_1$ electron energies ($\varepsilon(D_0)$) and ϕ_1 twising angles in varioius time intervals. Solid lines represent the linear correlation at the early stage of evolution.

the ϕ_2 twisting angle. The correlation between $\varepsilon(D_0)$ and ϕ_1 is weaker at times longer than 250 fs.

4. CONCLUSIONS

Using excited state isomerization dynamics simulation for ThT, we calculated the time resolved photoelectron spectra for 500 fs time delays. The calculated fluorescence intensity decays by 2 orders of magnitude upon ϕ_1 twisting within 400 fs, indicating that the subpicosecond fluorescence decay in unrestricted environments is mainly due to the twisting between benzothiazole and benzene groups. The subpicosecond fluorescence quenching of ThT in a restriction free environment does not necessarily indicate an internal conversion from S_1 to S_0. Photoelectron signals originate from channels from S_1 to excited ionized states decays in 100 fs due to the localization of wave functions caused by twisting. The $D_0 \leftarrow S_1$ feature decays much slower. The twisting angle ϕ_1 is related to the photoelectron spectra via two linear relations in the early stage of evolution, where the molecular twisting can be directly probed by the photoelectron signals with $\varepsilon \geq 1.0$ eV.

■ ASSOCIATED CONTENT

Supporting Information

Optimized S_0 and S_1 structures, and the time evolution of twisting angle ϕ_1 and energy levels for the trajectory used in Figure 5. This material is available free of charge via the Internet at http://pubs.acs.org.

■ AUTHOR INFORMATION

Corresponding Author

*E-mail: smukamel@uci.edu.

Notes

The authors declare no competing financial interest.

■ ACKNOWLEDGMENTS

We gratefully acknowledge the support of the National Institutes of Health (Grant R01 GM-59230), the National Science Foundation (Grant CHE-1058791), and the Chemical Sciences, Geosciences and Biosciences Division, Office of Basic Energy Sciences, Office of Science, U.S. Department of Energy (Grant DE-FG02-04ER15571). We acknowledge the computational resource support from the GreenPlanet cluster at UCI (NSF Grant CHE-0840513). B.P.F. gratefully acknowledges support from the Alexander-von-Humboldt Foundation through the Feodor-Lynen program.

■ REFERENCES

(1) Sipe, J. D.; Cohen, A. S. Review: History of the Amyloid Fibril. *J. Struct. Biol.* **2000**, *130*, 88−98.
(2) Chiti, F.; Dobson, C. M. Protein Misfolding, Functional Amyloid, and Human Disease. *Annu. Rev. Biochem.* **2006**, *75*, 333−366.
(3) Petkova, A. T.; Ishii, Y.; Balbach, J. J.; Antzutkin, O. N.; Leapman, R. D.; Delaglio, F.; Tycko, R. A Structural Model for Alzheimer's β-Amyloid Fibrils Based on Experimental Constraints From Solid State NMR. *Proc. Natl. Acad. Sci. U.S.A.* **2002**, *99*, 16742−16747.
(4) Caughey, B.; Lansbury, P. T., Jr. Protofibrils, Pores, Fibrils, and Neurodegeneration: Separating the Responsible Protein Aggregates from the Innocent Bystanders. *Annu. Rev. Neurosci.* **2003**, *26*, 267−298.
(5) Rishton, G. M. Aggregator Compounds Confound Amyloid Fibrillization Assay. *Nat. Chem. Biol.* **2008**, *4*, 159−160.
(6) Strasfeld, D.; Ling, Y.; Gupta, R.; Raleigh, D.; Zanni, M. Strategies for Extracting Structural Information from 2D IR Spectroscopy of Amyloid: Application to Islet Amyloid Polypeptide. *J. Phys. Chem. B* **2009**, *113*, 15679−15691.
(7) Shim, S.-H.; Gupta, R.; Ling, Y.; Strasfeld, D.; Raleigh, D.; Zanni, M. Two-Dimensional IR Spectroscopy and Isotope Labeling Defines the Pathway of Amyloid Formation with Residue-Specific Resolution. *Proc. Natl. Acad. Sci. U.S.A.* **2009**, *106*, 6614−6619.
(8) Singh, P.; Kumbhakar, M.; Pal, H.; Nath, S. Ultrafast Bond Twisting Dynamics in Amyloid Fibril Sensor. *J. Phys. Chem. B* **2010**, *114*, 2541−2546.
(9) Vassar, P. S.; Culling, C. F. Fluorescent Stains, with Special Reference to Amyloid and Connective Tissues. *Arch. Pathol.* **1959**, *68*, 487−498.
(10) Wolfe, L.; Calabrese, M.; Nath, A.; Blaho, D.; Miranker, A.; Xiong, Y. Protein-Induced Photophysical Changes to the Amyloid Indicator Dye Thioflavin T. *Proc. Natl. Acad. Sci. U.S.A.* **2010**, *107*, 16863−16868.
(11) Biancalana, M.; Makabe, K.; Koide, A.; Koide, S. Molecular Mechanism of Thioflavin-T Binding to the Surface of β-Rich Peptide Self-Assemblies. *J. Mol. Biol.* **2009**, *385*, 1052−1063.
(12) Stsiapura, V.; Maskevich, A.; Kuzmitsky, V.; Turoverov, K.; Kuznetsova, I. Computational Study of Thioflavin T Torsional Relaxation in the Excited State. *J. Phys. Chem. A* **2007**, *111*, 4829−4835.
(13) Stsiapura, V.; Maskevich, A.; Tikhomirov, S.; Buganov, O. Charge Transfer Process Determines Ultrafast Excited State Deactivation of Thioflavin T in Low-Viscosity Solvents. *J. Phys. Chem. A* **2010**, *114*, 8345−8350.
(14) Singh, P.; Kumbhakar, M.; Pal, H.; Nath, S. Confined Ultrafast Torsional Dynamics of Thioflavin-T in a Nanocavity. *Phys. Chem. Chem. Phys.* **2011**, *13*, 8008−8014.
(15) Stsiapura, V.; Maskevich, A.; Kuzmitsky, V.; Uversky, V.; Kuznetsova, I.; Turoverov, K. Thioflavin T as a Molecular Rotor: Fluorescent Properties of Thioflavin T in Solvents with Different Viscosity. *J. Phys. Chem. B* **2008**, *112*, 15893−15902.
(16) Singh, P.; Kumbhakar, M.; Pal, H.; Nath, S. Viscosity Effect on the Ultrafast Bond Twisting Dynamics in an Amyloid Fibril Sensor: Thioflavin-T. *J. Phys. Chem. B* **2010**, *114*, 5920−5927.
(17) Erez, Y.; Liu, Y.-H.; Amdursky, N.; Huppert, D. Modeling the Nonradiative Decay Rate of Electronically Excited Thioflavin T. *J. Phys. Chem. A* **2011**, *115*, 8479−8487.
(18) Stolow, A.; Bragg, A. E.; Neumark, D. M. Femtosecond Time-Resolved Photoelectron Spectroscopy. *Chem. Rev.* **2004**, *104*, 1719−1758.
(19) Hudock, H.; Levine, B.; Thompson, A.; Satzger, H.; Townsend, D.; Gador, N.; Ullrich, S.; Stolow, A.; Martínez, T. Ab Initio Molecular Dynamics and Time-Resolved Photoelectron Spectroscopy of Electronically Excited Uracil and Thymine. *J. Phys. Chem. A* **2007**, *111*, 8500−8508.
(20) Livingstone, R.; Schalk, O.; Boguslavskiy, A. E.; Wu, G.; Bergendahl, L. T.; Stolow, A.; Paterson, M. J.; Townsend, D. Following the Excited State Relaxation Dynamics of Indole and

5-Hydroxyindole Using Time-Resolved Photoelectron Spectroscopy. *J. Chem. Phys.* **2011**, *135*, 194307.
(21) Faubel, M.; Siefermann, K. R.; Liu, Y.; Abel, B. Ultrafast Soft X-ray Photoelectron Spectroscopy at Liquid Water Microjets. *Acc. Chem. Res.* **2012**, *45*, 120−130.
(22) Suzuki, T. Time-Resolved Photoelectron Spectroscopy of Non-Adiabatic Electronic Dynamics in Gas and Liquid Phases. *Int. Rev. Phys. Chem.* **2012**, *31*, 265−318.
(23) Lübcke, A.; Buchner, F.; Heine, N.; Hertel, I. V.; Schultz, T. Time-Resolved Photoelectron Spectroscopy of Solvated Electrons in Aqueous NaI Solution. *Phys. Chem. Chem. Phys.* **2010**, *12*, 14629−14634.
(24) Barbatti, M.; Granucci, G.; Persico, M.; Ruckenbauer, M. The On-the-Fly Surface-Hopping Program System Newton-X: Application to Ab Initio Simulation of the Nonadiabatic Photodynamics of Benchmark Systems. *J. Photochem. Photobiol., A: Chem.* **2007**, *190*, 228−240.
(25) Barbatti, M.; Granucci, G.; Ruckenbauer, M.; Plasser, F.; Pittner, J.; Persico, M.; Lischka, H. Newton-X: A Package for Newtonian Dynamics Close to the Crossing Seam, version 1.2. 2001; www.newtonx.org.
(26) TURBOMOLE V6.3 2011, A Development of University of Karlsruhe and Forschungszentrum Karlsruhe GmbH, 1989−2007, TURBOMOLE GmbH, since 2007; available from http://www.turbomole.com.
(27) Schriever, C.; Barbatti, M.; Stock, K.; Aquino, A.; Tunega, D.; Lochbrunner, S.; Riedle, E.; de Vivie-Riedle, R.; Lischka, H. The Interplay of Skeletal Deformations and Ultrafast Excited-State Intramolecular Proton Transfer: Experimental and Theoretical Investigation of 10-Hydroxybenzo[h]quinoline. *Chem. Phys.* **2008**, *347*, 446−461.
(28) Barbatti, M.; Aquino, A.; Lischka, H.; Schriever, C.; Lochbrunner, S.; Riedle, E. Ultrafast Internal Conversion Pathway and Mechanism in 2-(2′-Hydroxyphenyl)benzothiazole: A Case Study for Excited-State Intramolecular Proton Transfer Systems. *Phys. Chem. Chem. Phys.* **2009**, *11*, 1406−1415.
(29) Mitrić, R.; Werner, U.; Bonačić-Koutecký, V. Nonadiabatic Dynamics and Simulation of Time Resolved Photoelectron Spectra within Time-Dependent Density Functional Theory: Ultrafast Photoswitching in Benzylideneaniline. *J. Chem. Phys.* **2008**, *129*, 164118.
(30) Tapavicza, E.; Meyer, A. M.; Furche, F. Unravelling the Details of Vitamin D Photosynthesis by Non-Adiabatic Molecular Dynamics Simulations. *Phys. Chem. Chem. Phys.* **2011**, *13*, 20986−20998.
(31) Twenty-nine out of 36 trajectories survived from 500 fs evolution, which implies the multireference character is not important before 500 fs.
(32) Rahav, S.; Mukamel, S. Multidimensional Attosecond Photoelectron Spectroscopy with Shaped Pulses and Quantum Optical Fields. *Phys. Rev. A* **2010**, *81*, 063810.
(33) Melania, O. C.; Krylov, A. I. Dyson Orbitals for Ionization from the Ground and Electronically Excited States within Equation-of-Motion Coupled-Cluster Formalism: Theory, Implementation, and Examples. *J. Chem. Phys.* **2007**, *127*, 234106.
(34) Schuurman, M. S.; Weinberg, D. E.; Yarkony, D. R. On the Simulation of Photoelectron Spectra in Molecules with Conical Intersections and Spin-Orbit Coupling: The Vibronic Spectrum of CH3S. *J. Chem. Phys.* **2007**, *127*, 104309.
(35) Papas, B. N.; Schuurman, M. S.; Yarkony, D. R. The Simulated Photoelectron Spectrum of 1-Propynide. *J. Chem. Phys.* **2009**, *130*, 064306.
(36) Thompson, A. L.; Martnez, T. J. Time-Resolved Photoelectron Spectroscopy from First Principles: Excited State Dynamics of Benzene. *Faraday Discuss.* **2011**, *150*, 293−311.
(37) Rabalais, J. W. *Principles of UltraViolet Photoelectron Spectroscopy*; John Wiley and Sons: New York, 1977.
(38) Frisch, M. J.; et al. *Gaussian 09*, revision C.01; Gaussian Inc.: Wallingford, CT, 2009.
(39) Martin, R. L. Natural Transition Orbitals. *J. Chem. Phys.* **2003**, *118*, 4775−4777.